TENSOR-BASED SUBSPACE LEARNING FOR TRACKING SALT-DOME BOUNDARIES CONSTRAINED BY SEISMIC ATTRIBUTES

Zhen Wang, Zhiling Long, and Ghassan AlRegib

Center for Energy and Geo Processing (CeGP) at Georgia Tech and KFUPM,
Georgia Institute of Technology, Atlanta, GA 30332-0250, USA
{zwang313, zhiling.long, alregib}@gatech.edu

ABSTRACT

We propose a method to delineate salt-dome structures by tracking manually labeled boundaries through seismic volumes. We first extract texture features from boundary regions using the tensor-based subspace learning method. Then, we utilize one seismic attribute, the gradient of texture (GoT), as a constraint on the tracking process. Using texture features and GoT maps, we can identify tracked points and optimally connect them to synthesize the boundaries. The proposed method is evaluated using real-world seismic data and experimental results show that it outperforms the state of the art in accuracy, robustness, and computational efficiency.

Index Terms— salt dome tracking, texture, tensors, subspace learning, gradient of texture

1. INTRODUCTION

The evaporation of sea water leads to the deposition of salt. Salt grows upwards and commonly penetrates into surrounding rock strata, which leads to the formation of salt domes. Salt domes are mostly impermeable and can seal petroleum with surrounding strata. To localize petroleum reservoirs around salt domes, experienced interpreters need to accurately label salt-dome boundaries in migrated seismic data. With the dramatically growing size of collected seismic data, however, manual interpretation is becoming time consuming and label intensive. To speed up interpretation efficiency, in recent years, interpreters have been utilizing computer programs to interactively delineate salt-dome boundaries.

Since salt domes and their surrounding strata commonly have distinctive textures, to characterize the texture difference, salt-dome detection methods were proposed based on graph theory and image processing techniques. Lomask et al. [1] represented seismic sections as weighted undirected graphs. Based on the normalized cut image segmentation (NCIS) method, seismic sections can be partitioned into two parts along salt-dome boundaries. The NCIS-based method was later enhanced in [2] and [3]. Because of the high computational complexity of NCIS-based methods, Halpert et al. [4] employed a more-efficient graph-based segmentation method, referred to as "pairwise region comparison" [5], to delineate salt-dome boundaries. In recent years, edge detection operators such as 2D and 3D Sobel filters [6, 7] have also become a powerful tool for the detection of salt-dome boundaries. Since salt bodies have homogeneous textures in migrated seismic sections, Hegazy and AlRegib [8] proposed to combine three texture attributes (directionality, smoothness, and edge contents) to detect salt regions. More recently, Wang et al. [9] and Hegazy et al. [10] have described texture difference between the salt body and its neighboring rock strata in seismic sections using the GoT attribute. Shafiq et al. [11] enhanced the GoT attribute by analyzing the texture difference in the 3D space. In addition, methods based on the active contour [12] and machine learning [13, 14] have also been proved to be capable of detecting salt domes.

One main disadvantage of salt-dome detection methods is that interpreters need to tweak corresponding parameters for the best performance when dealing with different seismic sections. To overcome this drawback, Zhang and Halpert [15] proposed to track salt-dome boundaries using landmark-based shape deformation. In the work of [16], an energy function that involves the smoothness and continuity of the salt-dome boundary is used for tracking. More recently, Wang et al. [9, 17] proposed a tracking method using texture features extracted from the seismic section and its corresponding seismic attribute such as the GoT map or the contrast map of the gray level co-occurrence matrix (GLCM). However, these existing methods depend on only one reference section, which ignores the strong correlation between seismic sections. In this paper, we extract texture features from a group of seismic sections, which utilizes spatial correlation in all directions. The GoT map providing the necessary constraint can help increase the accuracy of tracked boundaries. According to the naming convention in video coding, we denote seismic sections with manually labeled boundaries as reference sections and the remaining ones as predicted sections.

2. THE PROPOSED METHOD

The block diagram of the proposed method is shown in Fig. 1. In following subsections, we are going to introduce each step in detail.

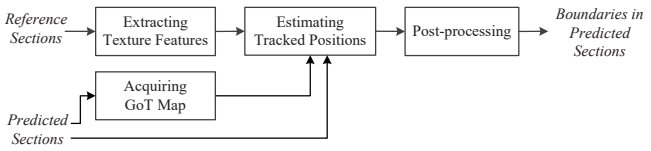

Fig. 1: The block diagram of the proposed method

2.1. Extracting Texture Features

On the basis of salt-dome boundaries labeled by interpreters in reference sections, we attempt to obtain texture features that involve spatial information on all directions. Tensors are commonly used to describe high dimensional ($N \geq 3$) data in the field of multi-linear algebra. For an N-th order tensor $\mathcal{A} \in \mathbb{R}^{I_1 \times I_2 \times \cdots \times I_N}$, each order represents a mode of $\mathcal{A}$. By unfolding $\mathcal{A}$ along the nth mode, we can obtain matrix $\mathbf{A}^{(n)} \in \mathbb{R}^{I_n \times (I_1 \times \cdots \times I_{n-1} \times I_{n+1} \cdots \times I_N)}$. The scalar product of tensor $\mathcal{A}, \mathcal{B} \in \mathbb{R}^{I_1 \times I_2 \times \cdots \times I_N}$, denoted $\langle \mathcal{A}, \mathcal{B} \rangle$, represents the sum of the products of corresponding entries in tensors. Based on the scalar product, the Frobenius norm of $\mathcal{A}$ is defined as $\|\mathcal{A}\|_F = \sqrt{\langle \mathcal{A}, \mathcal{A} \rangle} = \sqrt{\mathrm{Tr}(\mathbf{A}^{(n)} \cdot \mathbf{A}^{(n)^T})}$. The n-mode product of $\mathcal{A}$ and matrix $\mathbf{U} \in \mathbb{R}^{J_n \times I_n}$, denoted $\mathcal{A} \times_n \mathbf{U}$, defines new tensor $\mathcal{B}$, the entries of which are calculated as $\mathcal{B}(i_1 \cdots i_{n-1} j_n i_{n+1} \cdots i_N) = \sum_{i_n} \mathcal{A}(i_1 \cdots i_N) \cdot \mathbf{U}(j_n, i_n)$. This product can also be implemented by folding $\mathbf{U} \cdot \mathbf{A}^{(n)}$ along the nth mode.

In the proposed method, we build texture tensors from the labeled boundaries of reference sections. We define N_r neighboring seismic sections as reference sections, in which the corresponding boundaries, denoted $\mathbf{l}_b$, $b = 1, 2, \cdots, N_r$, are manually labeled. Points on these reference boundaries have the coordinate vectors of $\mathbf{l}_{b,k}$, $k = 1, 2, \cdots, K_b$, where K_b is the length of $\mathbf{l}_b$. To fully capture texture information along all reference boundaries, we focus on texture patches centered at boundary points with a size of $N_p \times N_p$. Therefore, third-order texture tensors can be built from these patches. To ensure the equality on both tracking directions, we first define the centers of texture tensors as points on the centric reference boundary $\mathbf{l}_{N_c}$, where $N_c = \lceil N_r/2 \rceil$. Then, to construct texture tensors, we need to identify the corresponding patch centers in neighboring reference sections. The localization of patch centers on $\mathbf{l}_b$, $b \neq N_c$, is shown as follows:

$$\tilde{\mathbf{l}}_{b,k} = \arg\min_{\mathbf{l}_{b,t}} \|\mathbf{l}_{b,t} - \mathbf{l}_{N_c,k}\|_2, t = 1, 2, \cdots, K_b. \quad (1)$$

Based on the definitions of $\mathbf{l}_{N_c}$ and Eq. (1), $\tilde{\mathbf{l}}_{N_c,k}$ is equal to $\mathbf{l}_{N_c,k}$. Therefore, boundary points on the centric section can identify groups of patch centers, denoted $\left\{\tilde{\mathbf{l}}_{b,k}, b = 1, 2, \cdots, N_r\right\}$, $k = 1, 2, \cdots, K_{N_c}$. By stacking texture patches belonging to the same group along the third direction as Fig. 2 shows, we can construct third-order texture tensors from reference sections, which are denoted as $\left\{\mathcal{A}_k \in \mathbb{R}^{N_p \times N_p \times N_r}, k = 1, 2, \cdots, K_{N_c}\right\}$.

Although current texture tensors contain texture information from all reference sections, only one tensor may not be enough to reflect the changes of textures along reference boundaries. Therefore, to utilize texture information along local boundaries, we introduce a tensor group centered at tensor $\mathcal{A}_k$, denoted $\mathcal{G}_k = \{\mathcal{A}_{k-N_s}, \cdots, \mathcal{A}_k, \cdots, \mathcal{A}_{k+N_s}\}$, where N_s determines the window size along boundaries. By applying the multi-linear principle component analysis (MPCA) [18] on $\mathcal{G}_k$, we can obtain projection matrices on each mode, denoted $\mathbf{U}_k^{(1)} \in \mathbb{R}^{J_{1,k} \times N_p}$, $\mathbf{U}_k^{(2)} \in \mathbb{R}^{J_{2,k} \times N_p}$, and $\mathbf{U}_k^{(3)} \in \mathbb{R}^{J_{3,k} \times N_r}$, where $J_{n,k}$, $n = 1, 2, 3$, are the dimensions of projected column subspace. By projecting $\mathcal{G}_k$ onto these matrices, we can obtain PCs, referred to as "texture features", in the form of tensors, denoted $\tilde{\mathcal{G}}_k$, which has the element calculated as follows:

$$\tilde{\mathcal{A}}_m = \mathcal{A}_m \times_1 \mathbf{U}_k^{(1)} \times_2 \mathbf{U}_k^{(2)} \times_3 \mathbf{U}_k^{(3)}, \quad m \in \{k - N_s, \cdots, k + N_s\}. \quad (2)$$

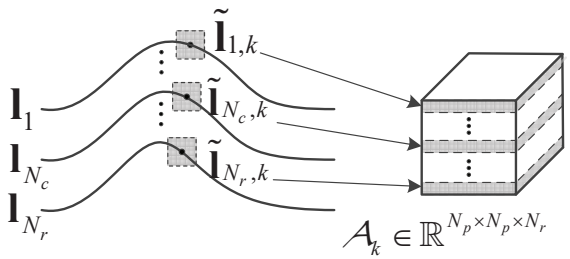

Fig. 2: The texture tensor built from the boundaries of reference sections

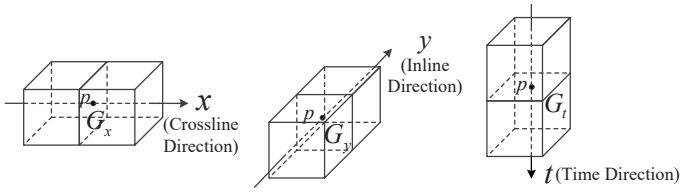

Fig. 3: Neighboring cubes defined around p in three directions

2.2. Acquiring GoT Maps

Using texture features extracted from reference boundaries, we can estimate the position of boundary points in predicted sections. However, migrated seismic data commonly involve noise, which may effect the accuracy of tracked boundary. Therefore, to increase the robustness of the tracking method, we select the GoT attribute [11] as a constraint because of its capability of describing the texture difference between the salt dome and its neighboring rock strata. For each point p in the predicted section, we define three pairs of cubes surrounding it as Fig. 3 shows. The texture difference between neighboring cubes represents the texture gradient along one direction, denoted G_i, $i \in \{x, y, t\}$. By combining these texture gradients, we can obtain the GoT value, which is calculated as $G = \sqrt{G_x^2 + G_y^2 + G_t^2}$. According to the work of [9, 11], texture gradients are consistent with the perception of inter-

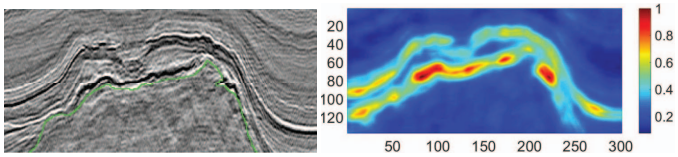

(a) Reference image (b) GoT map

Fig. 4: The reference image (inline 399) and its corresponding GoT map

preters and can be represented as follows:

$$G_i = E\left(\left|\mathscr{F}\left\{\left|\mathscr{F}\left\{\text{abs}\left(\mathbf{W}_{i-} - \mathbf{W}_{i+}\right)\right\}\right|\right\}\right|\right), i \in \{x, y, t\}, \quad (3)$$

where $|\mathscr{F}\{\cdot\}|$ represents the magnitude of 3D Fourier transform, $\{\mathbf{W}_{i-}, \mathbf{W}_{i+}\}$ defines the pair of neighboring cubes along one direction, and mean operator $E(\cdot)$ pools the difference cube into a single value. Fig. 4 shows one seismic section with the manually labeled salt-dome boundary in green and its corresponding GoT map. We notice that the blue area at the bottom of the GoT map roughly illustrates the salt body. In contrast, yellow and red regions indicate surrounding rock strata.

2.3. Estimating Tracked Positions

Using the GoT map and texture features extracted from reference boundaries, we can estimate the initial positions of tracked points. To ensure the computational efficiency of the tracking process, we project the labeled boundary of only the centric reference section onto the predicted section and keep the coordinates of all boundary points unchanged. To identify the optimal tracked position, we search along the normal direction of the projected point within a radius of $(2R_s + 1)$, where R_s is determined by the distance between the predicted section and the centric reference section. However, if the shape of the salt dome drastically changes among neighboring seismic sections, we may not be able to have access to the boundary area by searching around the current predicted point. Therefore, we need to shift projected points under the constraint of the GoT map. The shifting strategy with two thresholds is shown as follows:

$$\hat{\mathbf{l}}_{N_c,k} = \begin{cases} \tilde{\mathbf{l}}_{N_c,k} - R_s\mathbf{v}_\perp, & \bar{\mathbf{G}}\left(\tilde{\mathbf{l}}_{N_c,k}\right) > T_H \\ \tilde{\mathbf{l}}_{N_c,k} + R_s\mathbf{v}_\perp, & \bar{\mathbf{G}}\left(\tilde{\mathbf{l}}_{N_c,k}\right) < T_L \\ \tilde{\mathbf{l}}_{N_c,k}, & \text{Otherwise} \end{cases}, \quad (4)$$

where unit vector $\mathbf{v}_\perp$ indicates the normal direction of point $\tilde{\mathbf{l}}_{N_c,k}$ and $\bar{\mathbf{G}}\left(\tilde{\mathbf{l}}_{N_c,k}\right)$ represents the averaged GoT value of the 3×3 neighborhood of point $\tilde{\mathbf{l}}_{N_c,k}$. T_H and T_L defines two thresholds. If the averaged GoT value of $\tilde{\mathbf{l}}_{N_c,k}$ is greater than T_H, it means that the initially projected point is located in surrounding rock strata and needs to be shifted towards the salt body. In contrast, if the averaged GoT value of $\tilde{\mathbf{l}}_{N_c,k}$ is less than T_L, it means that the initially projected belongs to the salt body and needs to be shifted towards the boundary area.

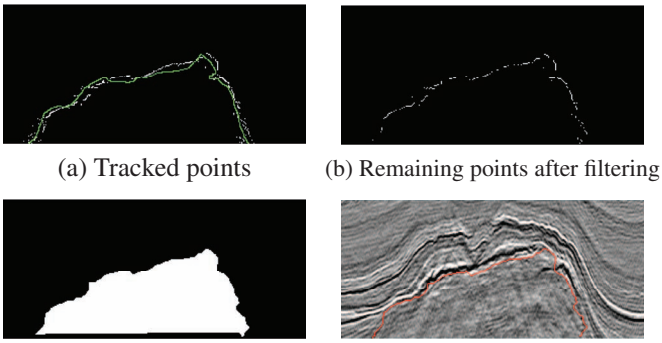

(a) Tracked points (b) Remaining points after filtering

(c) Highlighted salt body (d) Tracked boundary

Fig. 5: The post-processing steps to synthesize the tracked boundary

On the basis of projected point $\hat{\mathbf{l}}_{N_c,k}$, we define a group of potential tracked points, denoted $\hat{\mathbf{l}}^{(s)}_{N_c,k}$, $s = 1, 2, \cdots, (2R_s + 1)$. For each potential tracked point, we randomly select N_r points from its $\lceil\sqrt{N_r}\rceil \times \lceil\sqrt{N_r}\rceil$ neighborhood, which represent the centers of texture patches with a size of $N_p \times N_p$. By stacking these patches along the third direction, we can obtain texture tensor $\mathcal{P}^{(s)}_{N_c,k}$. As Eq. (2) shows, we extract the texture features of $\mathcal{P}^{(s)}_{N_c,k}$, denoted $\tilde{\mathcal{P}}^{(s)}_{N_c,k} \in \mathbb{R}^{J_{1,k} \times J_{2,k} \times J_{3,k}}$, using projection matrices $\left\{\mathbf{U}^{(1)}_k, \mathbf{U}^{(2)}_k, \mathbf{U}^{(3)}_k\right\}$. The difference between $\tilde{\mathcal{P}}^{(s)}_{N_c,k}$ and $\tilde{\mathcal{G}}_k$ can be calculated as follows:

$$d^{(s)}_{N_c,k} = \left\|\tilde{\mathcal{G}}_k - \tilde{\mathcal{P}}^{(s)}_{N_c,k}\right\|_F = \left(\sum \left\|\tilde{\mathcal{A}}_m - \tilde{\mathcal{P}}^{(s)}_{N_c,k}\right\|^2_F\right)^{1/2}. \quad (5)$$

The potential position with the smallest difference is the tracked position. Fig 5(a) illustrates the tracked points of the predicted section inline 389, which are estimated from the green labeled boundary of inline 399.

2.4. Post-processing

On the basis of tracked points, to synthesize the tracked boundary, we need to apply necessary post-processing steps. We first use the median filter to remove noisy points. By connection these remaining points shown in Fig. 5(d), we can highlight the salt body. To prevent from synthesizing the jagged boundary, we apply the closing operation on the highlighted salt body with a disk structuring element as Fig. 5(c) illustrates. The boundary extracted from Fig. 5(c) is shown in Fig. 5(d) as the tracked boundary in red.

3. EXPERIMENTAL RESULTS

In this paper, we apply the proposed salt-dome tracking method on a 3D real seismic dataset acquired from the

Netherlands offshore F3 block with the size of 24×16 km^2 in the North Sea [19]. To illustrate the performance of the proposed method, we focus on a local volume of the dataset containing discernible salt-dome structures. The tested volume has an inline number ranging from 389 to 409, a crossline number ranging from 401 to 701, and a time direction ranging from 1,300ms to 1,848ms with a step of 4ms. Figs. 4(a) and 5(d) illustrate seismic sections extracted from the local volume.

As we mentioned in previous sections, we first select seven reference sections with the inline number ranging from 396 to 402, the salt-dome boundaries in which are labeled by interpreters. Then we build texture tensors with a size of $20 \times 20 \times 7$ along labeled boundaries and extract texture features on the basis of Eq. (2). In the calculation of the GoT map, we define the size of cubes as $7 \times 7 \times 7$. In the tracking process, we empirically define T_H and T_L as 0.6 and 0.2, respectively. Search radius R_s is proportional to the offset between the predicted and the centric reference sections. In Fig. 6, we compare the green manually labeled ground truth with red tracked boundaries in inline 389 synthesized by the proposed method and the state-of-the-art method in [9], respectively. Fig. 7 shows the more details of the comparison in Fig. 6. We notice that the tracked boundary synthesized by the proposed method is more similar to the ground truth, in contrast to the one obtained in [9], especially around the left- and right-bottom. To objectively evaluate the similarity between tracked boundaries and the ground truth, we use the salSIM index proposed in [9], which is derived from the Frèchet distance [20]. In our experiment, we synthesize tracked boundaries in inline 389 to 395 and 403 to 409 using the proposed method and the method in [9]. We noticed that the salSIM index of boundaries synthesized by [9] has a decreasing trend with the increasing offset to the centric reference section. However, salt boundaries obtained by the proposed method yield more stable salSIM indices. Table 1 shows the statistics of the salSIM indices in Fig. 8, in which the averaged maximum distance (AMD) represents the mean of the Frèchet distance of the tracked boundaries to the ground truth. We implement both methods on a computer with Core i7-3720QM CPU at 2.60GHz and 12GB RAM and list the corresponding run-time in Table 1. We noticed that the proposed method has higher mean value, lower standard deviation, AMD, and computational complexity. In addition, the proposed method also has higher potential of being implemented in parallel, which can further increases interpretation efficiency.

4. CONCLUSION

In this paper, we proposed the method that tracks the boundaries of salt domes through seismic volumes using tensor-based subspace learning. We built texture tensors from a group of reference boundaries, which can capture spatial correlation in all directions. In addition, we proposed to utilize the GoT map as an important constraint in the tracking process. Experimental results showed that the proposed method outperforms the state-of-the-art in accuracy, robustness, and computational complexity.

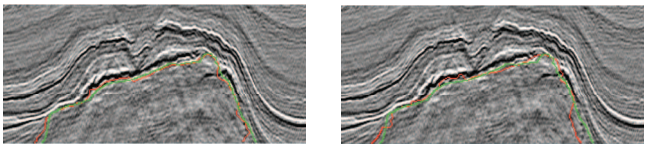

(a) (b)

Fig. 6: The comparison between the green ground truth and the red tracked boundaries of inline 389 synthesized by (a) the proposed method and (b) the tracking method in [9]

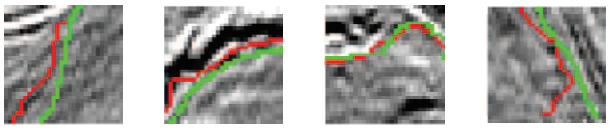

(a) Details of the tracked boundary in Fig. 6(a)

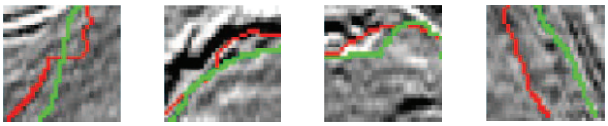

(b) Details of the tracked boundary in Fig. 6(b)

Fig. 7: The details of the green ground truth and the red tracked boundaries in Fig. 6

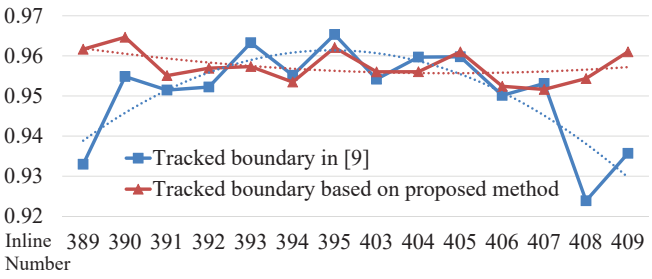

Fig. 8: The SalSIM indices of tracked boundaries ranging from 389 to 395 and 403 to 409

Table 1: The objective comparison between the proposed method and the tracking method in [9]

Tracking Method	Mean	Standard Deviation	AMD (pixel)	Elapsed CPU Time (s)
Proposed Method	0.9571	0.0041	7.86	44.84
Method in [9]	0.9508	0.0115	9.32	70.82

5. ACKNOWLEDGEMENTS

This work is supported by the Center for Energy and Geo Processing (CeGP) at Georgia Tech and by King Fahd University of Petroleum and Minerals (KFUPM).

6. REFERENCES

[1] Jesse Lomask, Biondo Biondi, and Jeff Shragge, "Image segmentation for tracking salt boundaries," in *Expanded Abstracts of the SEG 74th Annual Meeting*, 2004, pp. 2443–2446.

[2] Jesse Lomask, Robert G. Clapp, and Biondo Biondi, "Application of image segmentation to tracking 3D salt boundaries," *Geophysics*, vol. 72, no. 4, pp. P47–P56, 2007.

[3] Adam D. Halpert, Robert G. Clapp, and Biondo Biondi, "Seismic image segmentation with multiple attributes," in *Expanded Abstracts of the SEG 79th Annual Meeting*, 2009, pp. 3700–3704.

[4] Adam D. Halpert, Robert G. Clapp, and Biondo Biondi, "Speeding up seismic image segmentation," in *Expanded Abstracts of the SEG 80th Annual Meeting*, 2010, pp. 1276–1280.

[5] Pedro F. Felzenszwalb and Daniel P. Huttenlocher, "Efficient graph-based image segmentation," *International Journal of Computer Vision*, vol. 59, no. 2, pp. 167–181, 2004.

[6] Jing Zhou, Yanqing Zhang, Zhigang Chen, and Jianhua Li, "Detecting boundary of salt dome in seismic data with edge detection technique," in *Expanded Abstracts of the SEG 77th Annual Meeting*, 2007, pp. 1392–1396.

[7] Ahmed Adnan Aqrawi, Trond Hellem Boe, and Sergio Barros, "Detecting salt domes using a dip guided 3D Sobel seismic attribute," in *Expanded Abstracts of the SEG 81st Annual Meeting*, 2011, pp. 1014–1018.

[8] Tamir Hegazy and Ghassan AlRegib, "Texture attributes for detecting salt bodies in seismic data," in *Expanded Abstracts of the SEG 84th Annual Meeting*, 2014, pp. 1455–1459.

[9] Zhen Wang, Tamir Hegazy, Zhiling Long, and Ghassan AlRegib, "Noise-robust detection and tracking of salt domes in post-migrated volumes using texture, tensors, and subspace learning," *Geophysics*, accepted for publication.

[10] Tamir Hegazy, Zhen Wang, and Ghassan AlRegib, "The role of perceptual texture dissimilarity in automating seismic data interpretation," in *IEEE Global Conference on Signal and Information Processing (GlobalSIP)*, 2015.

[11] Muhammad A. Shafiq, Zhen Wang, Asjad Amin, Tamir Hegazy, Mohamed Deriche, and Ghassan AlRegib, "Detection of salt-dome boundary surfaces in migrated seismic volumes using gradient of textures," in *Expanded Abstracts of the SEG 85th Annual Meeting*, 2015, pp. 1811–1815.

[12] Muhammad A. Shafiq, Zhen Wang, and Ghassan AlRegib, "Seismic interpretation of migrated data using edge-based geodesic active contours," in *IEEE Global Conference on Signal and Information Processing (GlobalSIP)*, 2015.

[13] Asjad Amin and Mohammed Deriche, "A hybrid approach for salt dome detection in 2D and 3D seismic data," in *IEEE International Conference on Image Processing (ICIP)*, 2015.

[14] Asjad Amin, Mohammed Deriche, Tamir Hegazy, Zhen Wang, and Ghassan AlRegib, "A novel approach for salt-dome detection using a dictionary-based classifier," in *Expanded Abstracts of the SEG 85th Annual Meeting*, pp. 1816–1820.

[15] Yang Zhang and Adam D. Halpert, "Enhanced interpreter-aided salt boundary extraction using shape deformation," in *Expanded Abstracts of the SEG 82nd Annual Meeting*, 2012, pp. 1337–1341.

[16] Angélique Berthelot, Anne HS Solberg, Erlend Morisbak, and Leiv-J Gelius, "3D segmentation of salt using texture attributes," in *Expanded Abstracts of the SEG 82nd Annual Meeting*, 2012, pp. 1443–1447.

[17] Zhen Wang, Zhiling Long, and Ghassan AlRegib, "Tensor-based subspace learning for tracking salt dome boundaries," in *IEEE International Conference on Image Processing (ICIP)*, 2015.

[18] Haiping Lu, Konstantinos N Plataniotis, and Anastasios N Venetsanopoulos, "MPCA: Multilinear principal component analysis of tensor objects," *Neural Networks, IEEE Transactions on*, vol. 19, no. 1, pp. 18–39, 2008.

[19] Opendtect, "Netherland Offshore F3 Block Complete," `http://www.opendtect.org/index.php/share-seismic-data/osr.html`.

[20] Helmut Alt and Michael Godau, "Computing the Fréchet distance between two polygonal curves," *International Journal of Computational Geometry & Applications*, vol. 5, no. 01n02, pp. 75–91, 1995.